Direct Structural Determination by Inversion of Experimental Diffuse Low-Energy Electron Diffraction Intensities

C. M. Wei,[1] S. Y. Tong,[2] H. Wedler,[3] M. A. Mendez,[3,*] and K. Heinz[3]

[1]*Institute of Physics, Academia Sinica, Nankang, Taipei, Taiwan 11529, Republic of China*

[2]*Department of Physics and Laboratory for Surface Studies, University of Wisconsin-Milwaukee, Milwaukee, Wisconsin 53201*

[3]*Lehrstuhl für Festkörperphysik, Universität Erlangen-Nürnberg, Staudstrasse 7, D-91058 Erlangen, Germany*

(Received 27 September 1993)

We demonstrate that two-dimensionally resolved diffuse low-energy electron diffraction intensities can be measured with sufficient accuracy and at multiple energies to allow direct inversion for a low coverage (5%) disordered K/Ni(100) surface. The data inversion reveals three-dimensional coordinates of atoms with atom images whose full width at half maximum is less than 1 Å in all spatial directions. By varying the angle of incidence, first layer and second layer near-neighbor Ni atoms are separately imaged. This is the first demonstration of multiple-energy internal-source electron holography using measured elastically backscattered electrons.

PACS numbers: 68.35.Bs, 61.14.Hg, 61.16.−d, 68.55.−a

In the study of surface crystallography, a significant goal articulated in the early days of x-ray diffraction (1913) [1] and electron holography (1948) [2] has yet to be fulfilled. This goal is the ability to start with experimental intensity and invert the data to recover atomic positions without the intervention of theoretical modeling. Such a direct method bypasses the trial-and-error process whose success hinges on including the correct geometry as one of the trial structures. Recently, Saldin and de Andres [3] inverted theoretical diffuse low-energy electron diffraction (DLEED) intensities using a single-energy holographic wave front reconstruction method of Barton [4]. However, the presence of strong multiple scattering in the DLEED intensities and complex angular anisotropies in the reference wave [5–8] prevented single-energy inversion algorithms based on the optical holographic analog to produce useful information.

The purpose of this paper is to report the first successful inversion of experimental DLEED intensity to produce high-fidelity atom images whose configuration unambiguously fixes the surface geometry of the system studied. This system is Ni(001) with a 5% coverage of disordered K atoms. The method of DLEED data inversion is based on the scan-energy wave front reconstruction procedure of Wei and co-workers [6,9]. The relation between the scan-energy transform and other versions of multiple-energy electron-emission holography [10,11] has been discussed earlier [9]. Using measured intensities at multiple energies, the inversion of DLEED data produces bright spots whose full width at half maximum is less than 1 Å in *all spatial directions*. This is the first demonstration that two-dimensionally resolved DLEED intensities can be measured with sufficient accuracy and at multiple energies to allow direct inversion. Previous inversions of DLEED intensities at single energies did not obtain good resolution in the direction normal to the surface; there were also artifacts in the form of intense streaks at the origin [8].

For the present work, the configuration of the images shows that the K atom is adsorbed at a fourfold hollow site on Ni(001) with a vertical distance between 2.2 and 2.4 Å above the top Ni layer. This geometric information is non-model-dependent and it agrees with the structure determined by a trial-and-error method [12]. Furthermore, no in-plane K atom image is observed, indicating that the overlayer atoms at this coverage are dispersed. This result is also consistent with diffraction measurements [12].

The experiments are performed using a stainless steel UHV apparatus with a base pressure of less than 10^{-10} mbar. The Ni(100) crystal is of 0.99999 purity and oriented with an accuracy of better than $\pm 0.5°$. The main impurities, sulfur, carbon, and oxygen, are removed by repeated argon ion sputtering and subsequent annealing as described earlier [13] until no impurities can be detected by Auger electron spectroscopy. A sharp and low background LEED pattern is observed (Fig. 1, upper panel) and intensity vs energy spectra of the diffraction beams for this clean surface are measured and found to be practically identical to those reported in the literature [13–15]. Deposition of potassium is made at liquid nitrogen temperature using a commercially available dispenser.

For K coverages lower than 10% of a monolayer, diffuse intensities are observed to distribute over the whole LEED screen. Figure 1, lower panel, displays such a diffuse intensity distribution for a coverage of $\sim 5\%$ of a monolayer and a normal incident electron beam of 90 eV. The diffraction spots come from the well ordered Ni substrate. The intensity data are taken from the back of a spherical luminescent glass screen (opening angle 100°) by a video camera operated under computer control. This video LEED method [16,17] allows fast data acquisition with a rate of 20 msec for a full-screen intensity map. To improve the signal-to-noise ratio, each intensity is repeatedly measured 1024 times and subsequently averaged. This implies a total measuring time of only 20.5 sec for each final full-screen map. An image intensifier camera

0031-9007/94/72(15)/2434(4)$06.00

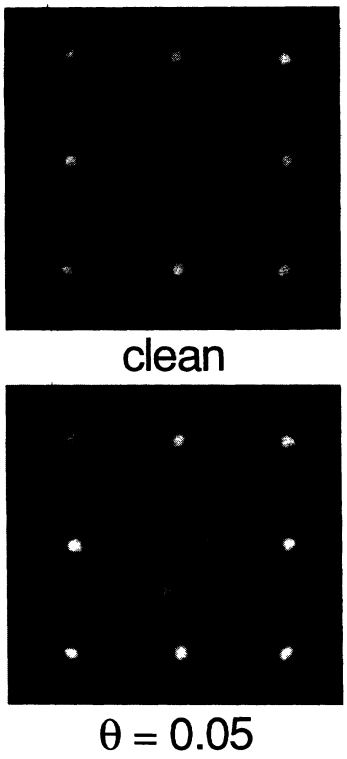

FIG. 1. Normal incidence intensity patterns of clean Ni(001) (upper panel) and 5% disordered K/Ni(001) (lower panel) at electron energy 90 eV. The electron gun's shadow is in the fourth quadrant.

is used to detect the weak diffuse intensities. The spatial resolution is 131×131 pixels per image. The intensity maps are taken from 90 to 303 eV, in a constant wave number grid of $\Delta k = 0.075$ a.u. for both normal incidence of the primary beam and oblique incidence with polar and azimuthal angles of $\theta = 35°$ from normal and $\phi = 22°$ from [100], respectively. The data are normalized for constant incident beam current. As will be seen in Figs. 4 and 5, it is not necessary to use the entire data range to obtain artifact-free atom images.

The low K coverage implies that the diffuse signal is weak, so diffuse signals caused by surface defects or quasielastic phonon scattering may not be negligible. Fortunately, it has been shown experimentally [18] and theoretically [19] that at low coverages, the phonon contributions are dominated by those of the clean substrate. Therefore, it is possible to get rid of phonon and defect contributions by separate measurements of the clean surface and subtracting the clean surface signal from that of the adsorbate system (for a survey, see Ref. [20]). This procedure is applied to each intensity map in the present work.

In Fig. 2, the upper panels show the difference maps K/Ni(001) − Ni(001) for two energies: from left to right, respectively, 90 and 96 eV. With submonolayer coverage of disordered K atoms, we expect the intensity at the substrate Bragg spots to weaken; therefore, the difference maps show holes (negative intensity values) near the Bragg spots. Typical intensity of the difference maps at non-Bragg positions ranges from 0 to 200, while at the holes the intensity is between 0 and −2000. At least two features concerning the difference maps are worth noting. First, the difference intensity at non-Bragg positions varies sensitively with energy. It is from this variation in the difference intensity that real space information is obtained. Second, the holes surrounding the Bragg spots contain no direct diffuse signal and these regions do not contribute to real space information. The same is true for the shadow areas of the electron gun and attachments. Because of a slightly inhomogeneous response of the luminescent screen, the difference maps do not show the expected C_{4v} symmetry even at normal incidence. Also, near the Bragg spots, the subtraction involves taking the difference of two very large numbers. As a result of slight changes in the electron gun's emission with and without K coverage, some residual signals are seen at or near the spots' center. However, the difference data away from the Bragg spots are only negligibly disturbed. It is necessary to eliminate the contributions from the intensity at the holes around the Bragg spots. We do this by replacing the intensity inside a circle of radius $r = 0.3g$ centered at each Bragg spot by the angular average of each difference map. Here $g = 2\pi/a$ is the length of the reciprocal basis vector of the square surface unit cell of Ni(001). When taking the angular average, all negative values (some are very large) are first set to zero. Typical values of the angular average range between 50 and 100. The choice of the cutoff radius is a compromise: Too big a cutoff radius results in discarding too much useful data; too small an r results in large discontinuities in the intensities inside and outside the circle.

The difference maps, with the holes at Bragg spots and negative intensity at the electron gun's shadow areas replaced by the angular averages, are shown in the lower panels of Fig. 2, respectively, for the same two energies. Examining the figure, we see that most of the useful data are preserved. The normal incidence data in the three quadrants not containing the shadow of the electron gun are then averaged and fourfold repeated before inversion. No further data processing is applied to the data before inversion.

In the inversion method of Wei and Tong [6], we Fourier transform the normalized scan-energy modulation with respect to vector position $\mathbf{R}$:

$$\phi_{\hat{\mathbf{k}}_f,\hat{\mathbf{k}}_i}(\mathbf{R}) = \int_{k_{\min}}^{k_{\max}} \chi(\mathbf{k}_f,\mathbf{k}_i) e^{-ikR} e^{i\mathbf{k}_f\cdot\mathbf{R}} dk \,. \quad (1)$$

In Eq. (1), the normalized modulation $\chi(\mathbf{k}_f,\mathbf{k}_i) = I(\mathbf{k}_f,\mathbf{k}_i)/I_A(\mathbf{k}_f,\mathbf{k}_i) - 1$, where $I(\mathbf{k}_f,\mathbf{k}_i)$ is the difference intensity shown in the lower panels of Fig. 2 and $I_A(\mathbf{k}_f,\mathbf{k}_i)$ is the least-square straight line fit to $I(\mathbf{k}_f,\mathbf{k}_i)$ in the $k_{\min} \le k \le k_{\max}$ range. We then sum the Fourier ampli-

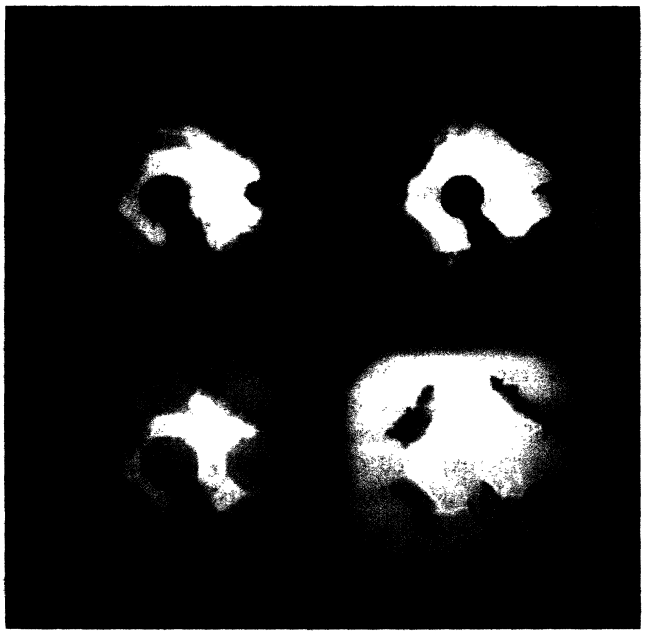

FIG. 2. Normal incidence difference K/Ni(001) − Ni(001) maps without (upper panels) and with (lower panels) angular average substitution.

tudes of Eq. (1) over different directions:

$$\phi_{\mathbf{k}_i}(\mathbf{R}) = \sum_{\mathbf{k}_f} \phi_{\hat{\mathbf{k}}_f,\hat{\mathbf{k}}_i}(\mathbf{R}) . \tag{2}$$

The real-space image is obtained by evaluating the absolute quantity $\mu_{\hat{\mathbf{k}}_i}(\mathbf{R}) = |\phi_{\hat{\mathbf{k}}_i}(\mathbf{R})|^2$. As demonstrated earlier from the inversion of calculated spectra [6], the wave number integral and summation over directions [Eqs. (1) and (2)] effectively eliminate artifacts due to multiple scattering and artifacts from the component of the reference wave which strikes the substrate atoms before scattering off the K atom. Also, the two-step process eliminates the requirement in traditional holographic reconstructions that the reference wave must be stronger than the object wave.

The two-step wave front reconstruction method [6,9] results in three-dimensional images of the near-neighbor atoms of the reference atom. We can display such images in different planes of view. Figure 3 shows a schematic diagram of the surface geometry determined by the images: The reference K atom is at a fourfold hollow site above the top layer Ni atoms [12]. The next-nearest neighbor atom Ni_5 is directly below the K atom. The image obtained from normal incidence data inversion is shown in Fig. 4. The figure shows a (010) plane of

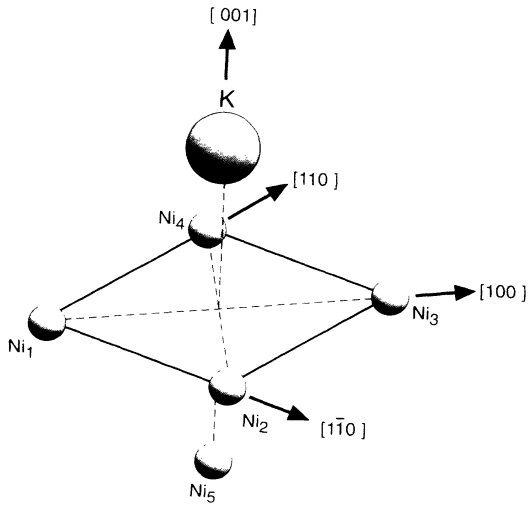

FIG. 3. Diagram of K adsorption site, showing nearest and next-nearest neighbor Ni atoms.

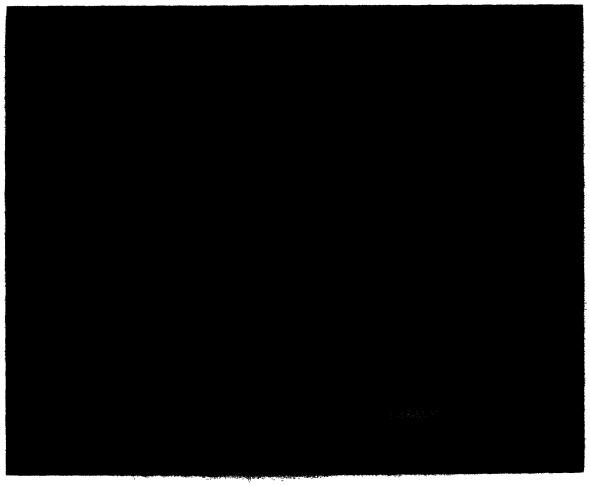

FIG. 4. Atom image from inverting normal incidence data: (010) plane of view passing through K. The bright spot is the image of Ni_5.

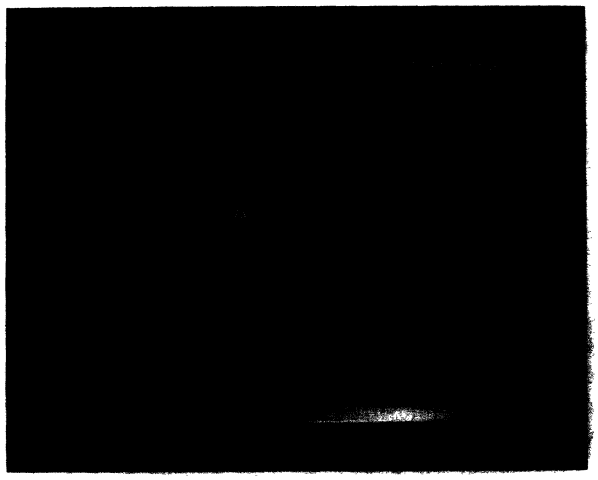

FIG. 5. Atom image from inverting off-normal incidence data: (010) plane of view passing through K. The bright spot is the image of Ni_1.

view which passes through the K, Ni_1, Ni_3, and Ni_5 atoms. A bright, high-resolution image of Ni_5 is seen. The crosses mark the reference K atom and the position of Ni_5 determined by diffraction [12]. The center of the image of Ni_5 is shifted by ~ 0.4 Å from the cross. The reason for the shift is nickel's scattering factor [21]. The very bright image of Ni_5 is due to forward focusing of the incident electron beam and the strong near 180° scattering of Ni_5 in the normal incidence geometry. The appearance of a substrate atom image directly behind the reference atom is predicted in the inversion of calculated normal-incidence DLEED spectra [6]. To overcome multiple scattering effects and eliminate artifacts due to other angular anisotropies, it is not necessary to use the entire data range: For normal-incidence data, the smallest energy range that produces an artifact-free image is 180–303 eV.

To view the other substrate atoms, we must use off-normal incidence data in a scattering geometry which enhances the backscattering of the other Ni atoms. The off-normal incidence data used here have an incident beam direction of $\theta = 35°$ from [001] and $\phi = 22°$ clockwise from [100]. Because the off-normal incidence data have no symmetry, we use only intensities within a quadrant bounded by the $[\bar{1}10]$ and $[\bar{1}\bar{1}0]$ directions. The difference maps K/Ni(001) − Ni(001) are determined from the experiment as before and angular averages are used to substitute difference values within circles with $r = 0.3$ g centered at Bragg spots. Therefore, except for not taking a fourfold average, the off-normal incidence data are processed identically as the normal incidence data. The image from inversion of off-normal incidence data (minimum data range required for an artifact-free image is 108–180 eV) is shown in Fig. 5. In Fig. 5, the plane of view is again (010) passing through the K, Ni_1, Ni_3, and Ni_5 atoms. However, in this scattering geometry, the backscattering from Ni_1 is most favored and, as expected, a bright image of Ni_1 is seen.

In conclusion, we have presented an experimental fulfillment of a long-standing goal of inverting elastically backscattered electron diffraction data to produce unambiguous surface structural information. Data acquisition of DLEED spectra is rapid (less than 21 sec per final screen) and data processing before inversion is kept to a minimum. A disadvantage of DLEED holography is that the reference wave is not chemically specific. Its advantage is that measurements can be made using laboratory-based apparatus. A potentially important usage of this direct method is uncovering low concentration adsorption sites. For example, searching through the three-dimensional (real) space, we find no image of in-plane K atoms [22]. This result indicates that the K atoms are adsorbed dispersely at fourfold hollow sites on Ni(001). Diffraction measurements, using indirect evidence, e.g., similarities between DLEED and LEED IV spectra, have reached the same conclusion [12]. We also envision systems in which the adsorbate atoms occupy different types of sites. Determination of the surface geometry in such systems by conventional diffraction methods is often difficult because of the large number of unknown parameters involved. Imaging by inversion of data can provide very useful direct information of such systems. Another use of the direct method is identifying off-symmetry adsorption sites. An example of this was given before using calculated spectra [23]. We are currently investigating this application of the direct method using measured DLEED spectra of disordered O on Ni(001).

C. W. Wei acknowledges the support of NSC, ROC, Grant No. 81-0208-M-001-75. S. Y. Tong acknowledges NSF Int-9011271 and DOE, Grant No. DE-FG02-84ER 45076. M. A. Mendez acknowledges the financial support of the Spanish government.

*On leave from Consejo Superior de Investigaciones Científicas, Madrid, Spain.

[1] W. L. Bragg, Proc. Cambridge Phil. Soc. **17**, 43 (1913).
[2] D. Gabor, Nature (London) **161**, 777 (1948).
[3] D. K. Saldin and P. L. de Andres, Phys. Rev. Lett. **64**, 1270 (1990).
[4] J. J. Barton, Phys. Rev. Lett. **61**, 1356 (1988).
[5] P. L. de Andres, Surf. Sci. **269/270**, 1 (1992).
[6] C. M. Wei and S. Y. Tong, Surf. Sci. Lett. **274**, L577 (1992).
[7] K. Heinz, R. Döll, M. Wagner, U. Löffer, and M. A. Mendez, Appl. Surf. Sci. **70/71**, 367 (1993).
[8] M. A. Mendez, C. Glück, J. Guerrero, P. L. de Andres, K. Heinz, D. K. Saldin, and J. B. Pendry, Phys. Rev. B **45**, 9402 (1992).
[9] S. Y. Tong, H. Huang, and C. M. Wei, Phys. Rev. B **46**, 2452 (1992).
[10] S. Y. Tong, Hua Li, and H. Huang, Phys. Rev. Lett. **67**, 3102 (1991).
[11] J. J. Barton, Phys. Rev. Lett. **67**, 3106 (1991).
[12] H. Wedler, M. A. Mendez, P. Bayer, U. Löffler, K. Heinz, V. Fritzsche, and J. B. Pendry, Surf. Sci. **293**, 47 (1993).
[13] W. Oed, H. Kindner, U. Starke, K. Heinz, K. Müller, and J. B. Pendry, Surf. Sci. **224**, 179 (1989).
[14] J. E. Demuth, P. M. Marcus, and D. W. Jepsen, Phys. Rev. B **11**, 1460 (1975).
[15] G. Hanke, E. Lang, K. Heinz, and K. Müller, Surf. Sci. **91**, 551 (1980).
[16] K. Heinz, Prog. Surf. Sci. **27**, 239 (1988).
[17] K. Müller and K. Heinz, in *The Structure of Surfaces*, Springer Series in Surface Science Vol. 2 (Springer, Berlin, 1986), p. 105.
[18] H. Ibach and S. Lehwald, Surf. Sci. **176**, 629 (1986).
[19] P. L. de Andres, P. J. Rous, and J. B. Pendry, Surf. Sci. **193**, 1 (1988).
[20] K. Heinz, Vacuum **41**, 328 (1990).
[21] S. Y. Tong, C. M. Wei, T. C. Zhao, H. Huang, and Hua Li, Phys. Rev. Lett. **66**, 60 (1991).
[22] J. G. Tobin, G. D. Waddill, H. Li, and S. Y. Tong, Phys. Rev. Lett. **70**, 4150 (1993).
[23] S. Y. Tong, H. Li, and H. Huang, Phys. Rev. B **46**, 4155 (1992).

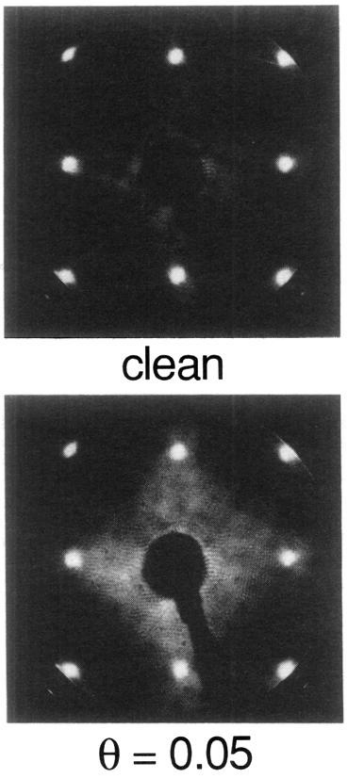

FIG. 1. Normal incidence intensity patterns of clean Ni(001) (upper panel) and 5% disordered K/Ni(001) (lower panel) at electron energy 90 eV. The electron gun's shadow is in the fourth quadrant.

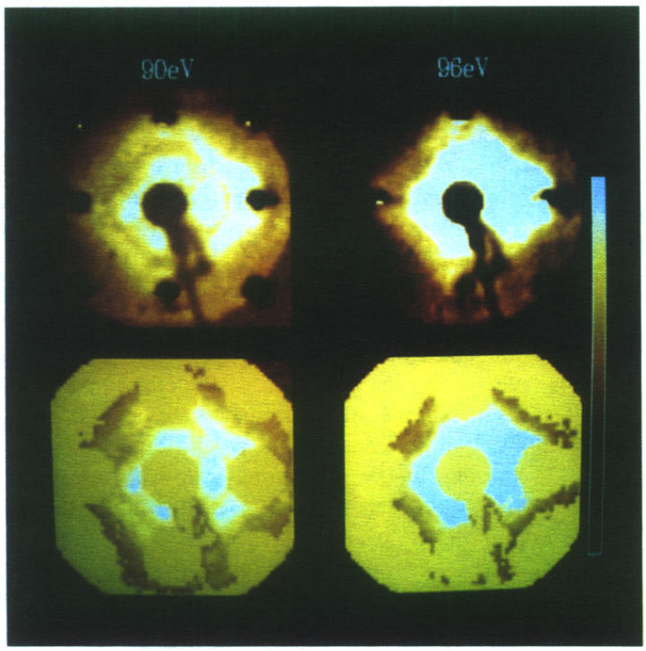

FIG. 2. Normal incidence difference K/Ni(001) − Ni(001) maps without (upper panels) and with (lower panels) angular average substitution.

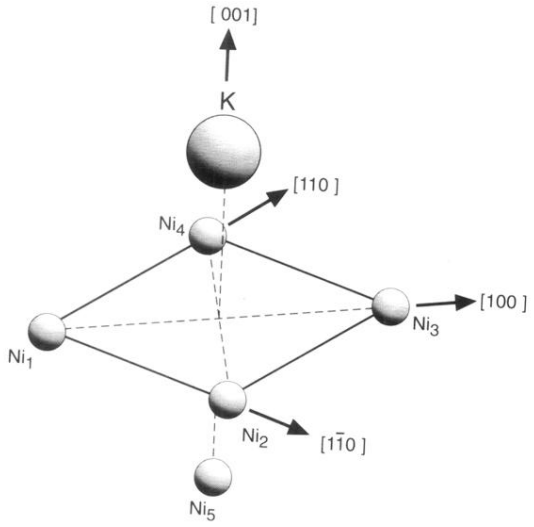

FIG. 3. Diagram of K adsorption site, showing nearest and next-nearest neighbor Ni atoms.

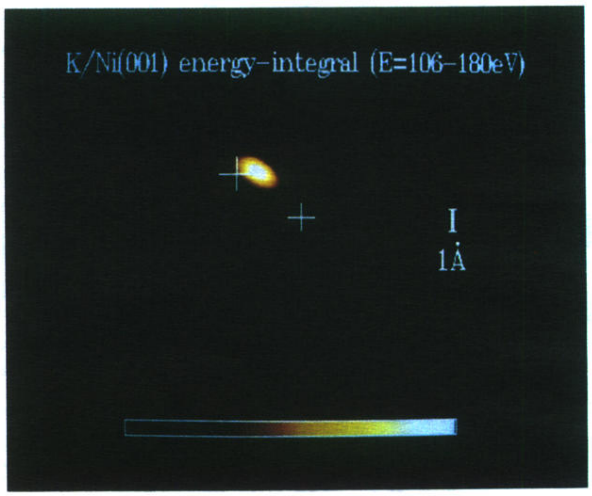

FIG. 4. Atom image from inverting normal incidence data: (010) plane of view passing through K. The bright spot is the image of Ni_5.

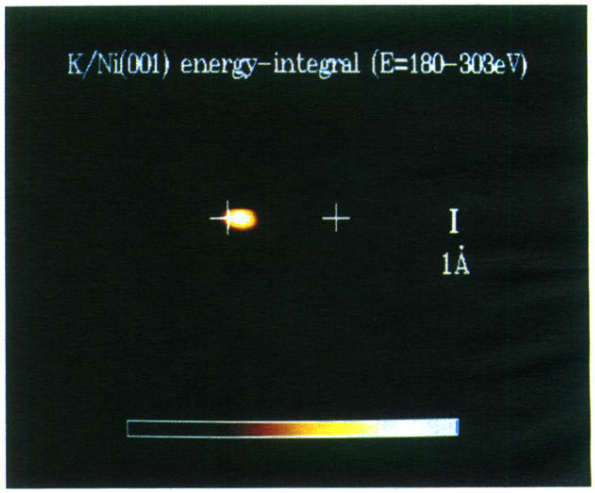

FIG. 5. Atom image from inverting off-normal incidence data: (010) plane of view passing through K. The bright spot is the image of Ni_1.